# Design of imaging keratometer with annular object and charge-coupled device detector

Yuanqing He,[1,2] Yan Wang,[3,*] Zhaoqi Wang,[1,2] Yao Wang,[4] Yongji Liu,[1,2] Lin Zhang,[3] Yi Zhai,[1,2] and Shengjiang Chang[1,2]

[1]Institute of Modern Optics, Nankai University, Tianjin 300071, China

[2]Key Laboratory of Optical Information Science and Technology, Ministry of Education, Tianjin 300071, China

[3]Tianjin Eye Hospital & Eye Institute, Tianjin Key Lab of Ophthalmology and Visual Science, Tianjin Medical University, Tianjin 300020, China

[4]Changchun Institute of Optics, Fine Mechanics and Physics, Chinese Academy of Science, Changchun 130033, China

*Corresponding author: wangyan7143@vip.sina.com

Received 19 August 2013; revised 4 November 2013; accepted 5 November 2013; posted 6 November 2013 (Doc. ID 195818); published 6 December 2013

A novel imaging keratometer by the aid of modern optoelectronic technology is proposed. The optical system consists of an annular object, a first imaging subsystem, a second imaging subsystem, and a CCD detector. The measurement range of corneal refraction is from 30D to 60D (5.5–11 mm in radius of curvature), and the accuracy reaches 0.156D, 0.072D, and 0.036D, respectively, for the corneal surface of the steepest, the radius of curvature of 7.8 mm, and the corneal surface of the flattest. The accuracy of corneal astigmatism is verified to be 0.05D for cylindrical refraction of 0.75D. Compared with the traditional keratometer, the proposed keratometer possesses advantages of high accuracy. 

*OCIS codes:* (330.7327) Visual optics, ophthalmic instrumentation; (120.3890) Medical optics instrumentation.

http://dx.doi.org/10.1364/AO.52.008532

## 1. Introduction

Since the successful measurement of wavefront aberrations of human eyes at the end of the last century [1], wavefront technology has advanced considerably in the development of ophthalmic and relevant areas. The customized laser ablation of cornea guided by wavefront aberrations has become an increasingly popular surgery [2,3]. A spectacle lens with refractive power determined by wavefront data, the objective refraction, has been devised [4,5]. Thibos *et al.* reported that the accuracy to predict the refraction error of the spherical component by objective refraction was within 0.125D [6]. He *et al.* investigated the contributions of both the anterior corneal surface and the internal optics of eyes to lower-order aberrations and to higher-order aberrations [7]. Guo *et al.* constructed an individual eye model with measurements of wavefront aberrations and corneal topography [8]. Apparently, as the measurement accuracy of the eye's wavefront aberrations grows higher, the measurement accuracy of the corneal surface should be correspondingly improved. The corneal surface is the most powerful refraction element of the eyeball, providing 2/3 of the total refraction. Measurement of the refractive power of the cornea is essential for patients undergoing refractive surgery or visual correction with contact lenses [9].

The traditional keratometer generally adopts double image prisms to measure the corneal refraction, and the accuracy is normally 0.25D [10]. The

1559-128X/13/358532-08$15.00/0

accuracy is defined as the minimum variation of refraction that the apparatus can distinguish in measurement. The Bausch & Lomb keratometer is a one-position manual keratometer, with fixed object and variable image. It employs an image doubling by means of axially movable horizontal and vertical prisms. From the product description, the measurement accuracy is 0.12D. Manual operation inevitably introduces subjective error, and the operator's proficiency in the measurement is required. The Orbscan corneal topography system is an optical-based, slit scanning instrument that measures three-space points on the corneal surfaces [11]. With this apparatus, the measurement accuracy of corneal refraction is about 0.25D [12]. The Pentacam is a rotating Scheimpflug camera, and the rotational measuring procedure generates Scheimpflug images. It calculates a three-dimensional model of the anterior eye segment from 25,000 true elevation points [13], and the accuracy of corneal refraction is about 0.2D according to the product description.

In this paper a novel imaging keratometer with an annular object and a CCD detector is proposed. A corresponding optical system that consists of first and second imaging subsystems is designed. By the aid of modern optoelectronic imaging technology and image processing technology, the proposed keratometer has high accuracy and a wide measurement range.

## 2. Methods

### A. Principles

The anterior corneal surface is characterized as approximately spherical within the central optical zone, and gradually flattening at the periphery. Therefore the illumination area at the corneal surface of the keratometer should be controlled in a central zone ranging from 1 to 2 mm in radius for different corneal curvatures. In this way the measurement results are more reliable. Figure 1 is a schematic diagram of the optical system of the proposed keratometer, which consists of first and second imaging subsystems. The first imaging subsystem forms a first middle image of the annular object at a certain distance behind the corneal surface, and the corneal surface forms a second middle image at a shorter distance behind the corneal surface. The second imaging subsystem forms the final image on the CCD detector. The spherocylindrical refraction of the corneal surface is obtained by computer analysis of the acquired digital annular image.

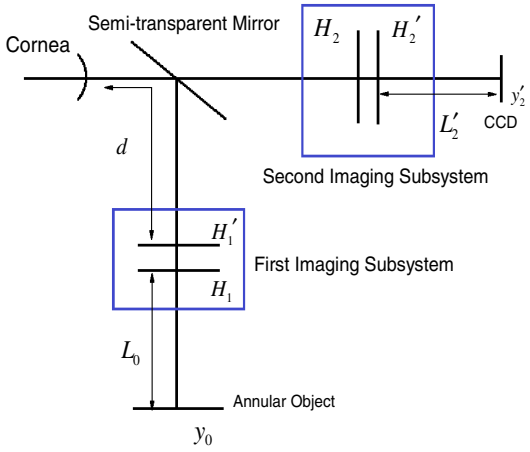


Fig. 1. Schematic diagram of the keratometer's optical system.

We assume that the height of the annular object is $2y_0$, the distance between the object and the principal plane $H_1$ is $L_0$, the effective focal length and magnification are $f_1$ and $\beta_1$, respectively, the radius of curvature of the corneal surface is $r$, the distance between the corneal surface and the principal plane $H_1'$ is $d$, the effective focal length and magnification of the second imaging subsystem are $f_2$ and $\beta_2$, respectively, the height of the annular image on the CCD detector is $2y_2'$, and the distance between the image plane and the principal plane $H_2'$ is $L_2'$. In terms of the lens equation, magnification equation, and mirror equation, the radius of curvature of the corneal surface can be expressed as

$$r = \frac{2(\beta_1 L_0 - d)}{1 + \frac{\beta_1 \beta_2 y_0}{y_2'}}, \tag{1}$$

$$\beta_1 = \frac{f_1}{f_1 + L_0}, \tag{2}$$

$$\beta_2 = \frac{f_2 - L_2'}{f_2}. \tag{3}$$

The optical system has an external focusing model, by adjusting the distance of $L_2'$, and we note that the magnification of the second imaging subsystem $\beta_2$ varies along with the radius of curvature of the cornea surface. The refractive power of the corneal surface can be then determined by

$$P = \frac{1000(n-1)}{r}, \tag{4}$$

where $P$ is the refractive power in the diopter, $n$ is the refractive index of the cornea, and $r$ is the radius of curvature of the corneal surface in millimeters.

Corneal astigmatism is determined by the difference in refractive power between two principal meridians of the corneal surface, which have maximum and minimum refractive power, respectively. During focusing adjustment, the annular object can be focused only along a certain radial direction but blurred along others, at two specific planes with different distances of $L_2'$. The shorter distance corresponds to the focusing plane of the principal meridians of the corneal surface with maximum refractive power, and another corresponds to that with minimum refractive power. The focusing radial directions are different at the two planes, and they

are perpendicular with each other in the case of regular astigmatism. The focusing can be realized by means of autofocusing based on image processing [14]. It is assumed that well-focused images have more high-frequency content than defocused images, and neighboring pixels in images with high-frequency content have large differences in intensity. The larger the intensity changes, the sharper the edges. Thus the focusing in radial directions can be obtained by using the differential operator of the image in radial directions. We assume that the radii of annular images in the focusing directions at the two planes are $y'_{2,1}$ and $y'_{2,2}$, respectively, and the magnifications of the second imaging subsystem are $\beta_{2,1}$ and $\beta_{2,2}$, respectively. With Eq. (1), the radii of curvature of the corneal surface in two principal meridians can be expressed as

$$r_1 = \frac{2(\beta_1 L_0 - d)}{1 + \frac{\beta_1 \beta_{2,1} y_0}{y'_{2,1}}}, \tag{5}$$

$$r_2 = \frac{2(\beta_1 L_0 - d)}{1 + \frac{\beta_1 \beta_{2,2} y_0}{y'_{2,2}}}. \tag{6}$$

Then the radii of curvature of $r_1$ and $r_2$ are converted to reflective powers $P_1$ and $P_2$ with Eq. (4), and the astigmatism can be written as

$$C = P_1 - P_2. \tag{7}$$

### B. Design of the Optical System

The optical system of the imaging keratometer is designed with ZEMAX software. We set the external and internal radii of the annular object to be 5 and 4.6 mm, respectively, and the working wavelength to be 850 nm. The CCD detector is with pixels of $1280 \times 960$, and pixel size of $3.75\ \mu m \times 3.75\ \mu m$. So the Nyquist limitation of the system is 133 lp/mm. The illumination area on the corneal surface should be controlled in a central zone ranging from 1 to 2 mm in radius. This is a constraint condition of the numerical aperture of the optical system. Table 1 shows the specific parameters of the design.

#### 1. *First Imaging Subsystem*

The first imaging subsystem projects rays from the annular object on the corneal surface. Considering the constraint of illumination area on the corneal surface, the magnification of the subsystem should be less than 1 to ensure the formed image is smaller than the illumination area. The image plane should be located at a certain distance, 20 mm for instance, behind the corneal surface. Otherwise, rays reflected by the corneal surface will have a larger divergent angle, which makes the design of the second imaging subsystem more difficult. Furthermore, the working distance of the system, the distance between the corneal surface and the inserted semitransparent mirror, should be relatively long to ensure a proper measurement condition of eyes.

**Table 1. Specific Parameters of Design**

| | |
|---|---|
| Wavelength | 850 nm |
| External and internal radii of annular object | 5 mm, 4.6 mm |
| Measurement range of corneal surface | 5.5–11 mm in radius of curvature |
| Accuracy | 0.08D (for $r = 7.8$ mm) |
| Target surface size of CCD | $4.8\ mm \times 3.6\ mm$ |
| Resolution of CCD | $1280 \times 960$ |
| Pixel size | $3.75\ \mu m \times 3.75\ \mu m$ |
| Illumination area on corneal surface | 1–2 mm in radius |

The first imaging subsystem is designed based on a double Gauss structure that contains six lenses. The double Gauss lens has a nearly symmetric arrangement of elements about a central stop with the characteristics of high numerical aperture, high resolution, and low distortion. According to the specific parameters of the design, we set the object half-height to be 5 mm (the external radius of the annular object), the effective focal length to be 70 mm, the distance between the object and the first surface to be 150 mm, and the back working distance to be 80 mm. The half-height of the image is 2.83 mm, and the magnification is 0.566. Figure 2(a) is the layout of the first imaging subsystem, and Table 2 shows the structural parameters in detail.

#### 2. *Second Imaging Subsystem*

The first imaging subsystem forms the first middle image with half-height of 2.83 mm behind the corneal surface. In the case of the flattest corneal surface ($r = 11$ mm), the corneal surface forms a second middle image with half-height of 1.08 mm. Considering that the size of the CCD target is 1.8 mm in half-height, the magnification of the second imaging subsystem should be 1.66 to ensure the target surface is fully utilized. The second imaging subsystem designed is also a double Gauss system with seven lenses. The effective focal length is 84 mm, and the magnification is 1.66. It is noticed that the image distance of the second imaging subsystem varies with the radius of curvature of the corneal surface. Figure 2(b) is the layout of the second imaging subsystem, and Table 3 shows the structural parameters in detail

#### 3. *Optical System of Imaging Keratometer*

Figure 2(c) is the layout of the optical system of the imaging keratometer. Two subsystems are connected by a semitransparent mirror. The second middle image formed by the corneal surface acts as the object of the second subsystem.

To acquire precise spherocylindrical refraction of the corneal surface, aberrations, especially the astigmatism of the optical system, should be eliminated. The penultimate surface of the first imaging

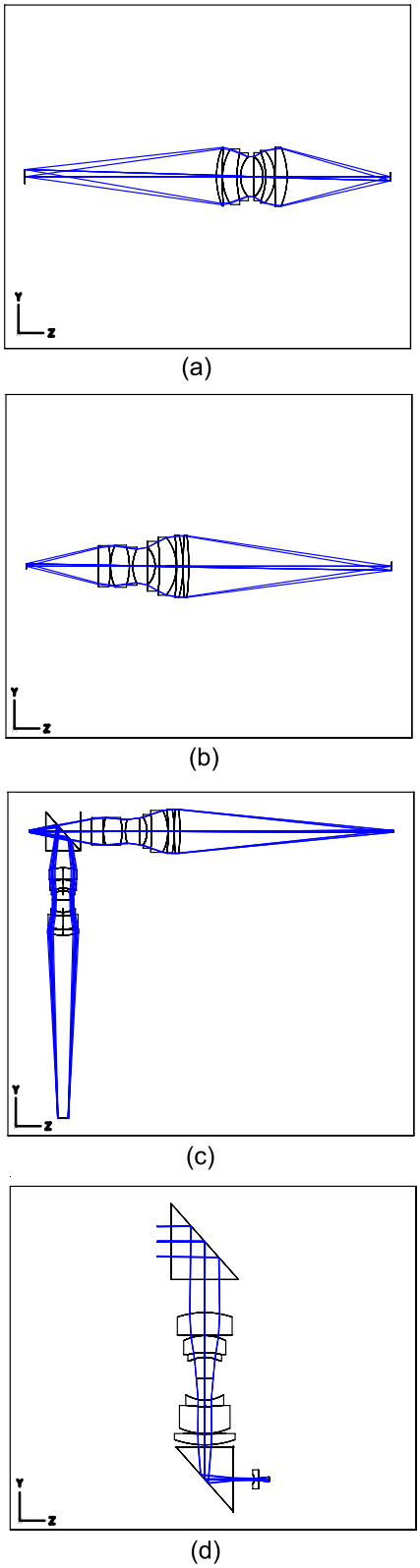


Fig. 2. Layout of (a) first imaging subsystem, (b) second imaging subsystem, (c) imaging keratometer's optical system, and (d) alignment system.

subsystem is therefore set as the "biconic" type in ZEMAX to eliminate the intrinsic astigmatism of the system, and the last surface is set as the

**Table 2. Structural Parameters of First Imaging Subsystem**

| Surface | Radius | Thickness | Glass |
|---|---|---|---|
| Object | Infinity | 150.000 | |
| 1 | 48.426 | 4.568 | LAFN23 |
| 2 | 284.072 | 0.208 | |
| 3 | 32.600 | 11.315 | LAF2 |
| 4 | 68.243 | 2.740 | SF1 |
| 5 | 19.061 | 10.394 | |
| Stop | Infinity | 7.209 | |
| 7 | −17.639 | 1.990 | SF13 |
| 8 | −38.120 | 7.111 | LAF2 |
| 9 | −24.870 | 0.198 | |
| 10 | 876.232 | 9.540 | LAFN21 |
| 11 | −45.835 | 80.85 | |
| Image | Infinity | 0 | |

**Table 3. Structural Parameters of Second Imaging Subsystem**

| Surface | Radius | Thickness | Glass |
|---|---|---|---|
| Object | Infinity | 65.000 | |
| 1 | 449.037 | 10.860 | LAKN12 |
| 2 | −92.559 | 0.200 | |
| 3 | 36.911 | 16.920 | BAF51 |
| 4 | −44.286 | 3.130 | SF8 |
| 5 | 27.943 | 13.022 | |
| Stop | Infinity | 7.027 | |
| 7 | −19.829 | 4.140 | FN11 |
| 8 | −150.874 | 15.050 | LAFN28 |
| 9 | −33.451 | 0.200 | |
| 10 | −219.441 | 5.760 | LASFN30 |
| 11 | −87.416 | 0.200 | |
| 12 | 323.138 | 4.950 | SK10 |
| 13 | −190.255 | 182.962 | |
| Image | Infinity | 0 | |

"aspheric" type to correct the spherical aberration and other aberrations. To accommodate patients with different corneal refractions, we set multiconfigurations corresponding to radii of curvature of corneal surfaces in a range of 5.5–11 mm, and perform optimization of the whole optical system. The optical system is of the external focusing model with the CCD detector being translated along the optical axis. In this way, the radius of the annular image, along with the position of the image plane (CCD), varies with the radius of curvature of the corneal surface correspondingly. Results show that high measurement accuracy can be obtained by the designed optical system.

### 4. *Alignment System*

An alignment system is designed as shown in Fig. 2(d). An emitted crossed target (object) and a concave lens are placed at proper position of the apparatus, with the image of the crossed target at infinity. The working wavelength is set to be 650 nm. During the measurement, subjects are asked to stare at the fixation target to ensure the visual axis of the eye is coincident with the optical axis of the imaging system.

## 3. Results

The measurement range of the radii of curvature of anterior corneal surfaces is from 5.5 to 11 mm, and it is 7.8 mm in the Gullstrand–Le Grand eye model [15]. Thus we take 5.5, 7.8, and 11 mm as the referential radii of curvature to analyze the performance of the optical system. Figure 3 shows the MTF curves of the optical system corresponding to the above three radii of curvature. The blue and green curves represent the object half-height of 4.6 and 5 mm, receptively, and the black curve represents the diffraction limit. It can be seen that the MTF curves are close to those of diffraction limit, with value greater than 0.2 at the spatial frequency of 133 cycles/mm. This implies that the optical system has a satisfactory imaging performance in the measurements of corneas with different radii of curvature.

To simulate the illumination of the annular image on the CCD, the imaging system, together with aberrations of the system, is transferred from Zemax to TracePro. The annular object is modeled as a Lambertian source at wavelength of 850 nm, with an output power of 5 mW. Figure 4 shows an irradiance color map at the image plane provided by TracePro software.

The radius of the annular image is calculated by the centroid algorithm from luminous intensities of pixels (1024 × 1024) on the image surface. Figure 5 is the schematic diagram of the calculation. We set a coordinate system with the geometric center of annulus as the origin, and calculate the radius in different radial directions as follows:

$$\bar{X}_{\theta_i} = \frac{\sum x_i l(x_i, y_i)}{\sum l_i(x_i, y_i)}, \tag{8}$$

$$\bar{Y}_{\theta_i} = \frac{\sum y_i l(x_i, y_i)}{\sum l_i(x_i, y_i)}, \tag{9}$$

$$\bar{R}_{\theta_i} = \sqrt{\bar{X}_{\theta_i}^2 + \bar{Y}_{\theta_i}^2}, \tag{10}$$

where $(x_i, y_i)$ is the position of one pixel in the radial direction of $\theta_i$, $l(x_i, y_i)$ is the luminous intensity of

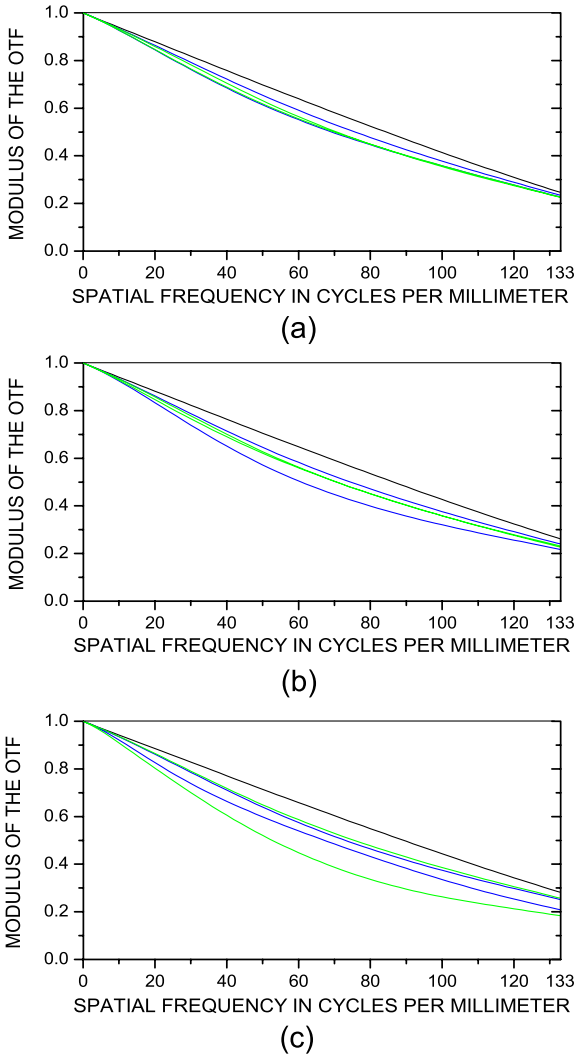


Fig. 3. MTF curves of imaging system corresponding to different radii of curvature of corneal surfaces. (a) $r = 5.5$ mm, (b) $r = 7.8$ mm, and (c) $r = 11$ mm.

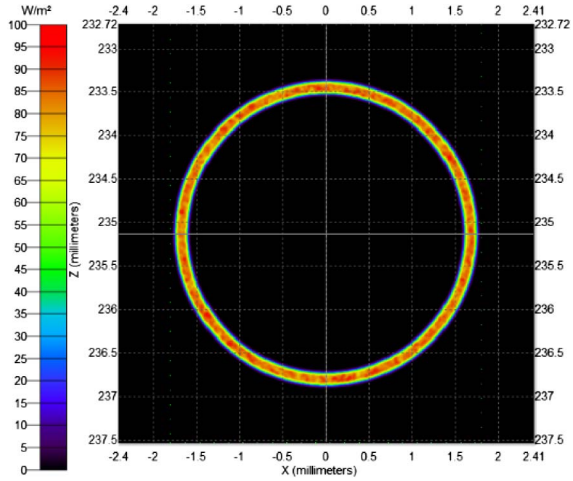


Fig. 4. Irradiance color map of the image surface.

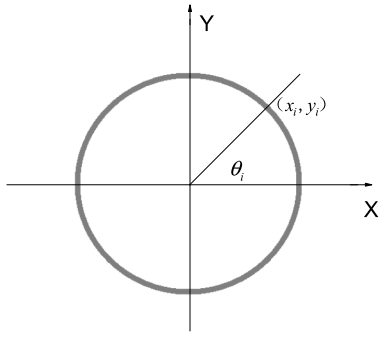


Fig. 5. Schematic diagram of calculating the radius of annulus by the centroid algorithm

Table 4. Radius of Annular Image ($R$) Calculated by Centroid Algorithm for Different Radius of Curvature ($r$) of Corneal Surface

| | | | | | | |
|---|---|---|---|---|---|---|
| $r$(mm) | 5.5 | 6 | 6.5 | 7 | 7.5 | 7.8 |
| $R$(mm) | 0.7738 | 0.8525 | 0.9288 | 1.0092 | 1.0894 | 1.1363 |
| $r$(mm) | 8.3 | 9 | 9.5 | 10 | 10.5 | 11 |
| $R$(mm) | 1.2184 | 1.3341 | 1.4187 | 1.5052 | 1.5917 | 1.6787 |

this pixel, $(\bar{X}_{\theta_i}, \bar{Y}_{\theta_i})$ is the position of the centroid in the radial direction of $\theta_i$, and $R_{\theta_i}$ is the radius of annulus in this direction. The radius of annulus can be expressed as

$$R = \frac{\sum_1^m \bar{R}_{\theta_i}}{m}, \tag{11}$$

where $m$ is the number of radial directions. The calculating procedure is implemented with MATLAB.

The radius of the annular image varies as the radius of curvature of the corneal surface. We calculate 12 radii of annular images corresponding to 12 radii of curvature of corneal surfaces in a range from 5.5 to 11 mm. Results are listed in Table 4. The standard deviation of the radii in different radial directions is quite low. As the radius of curvature of the corneal surface is 5.5 mm, the standard deviation in different directions is 2.07 μm, and it is, respectively, 1.95 and 1.52 μm as the radii of curvature are 7.8 and 11 mm. This implies that for the corneal surface without astigmatism, the radius of the annular image can be calculated in an arbitrary radial direction, and the standard deviation of 2.1 μm can be considered as the minimum variation of the radius of the annular image that can be detected.

The relationship between the radius of curvature of the corneal surface and the radius of the annular image is plotted in Fig. 6 according to the data in Table 4. The abscissa indicates the radius of curvature, while the ordinate indicates the radius of the annular image. It can be used as the calibration

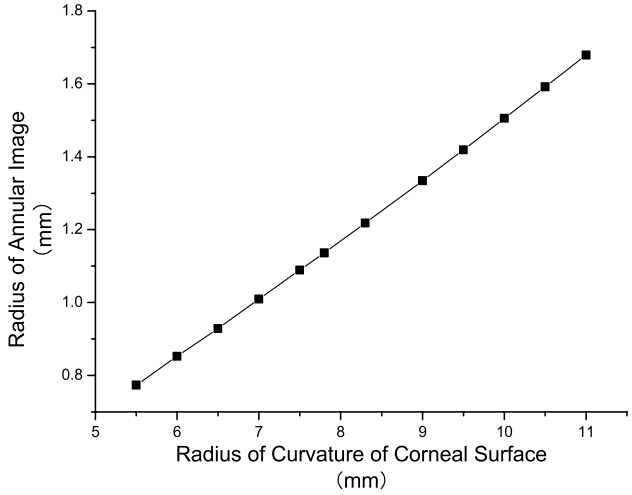


Fig. 6. Relevance between the radius of curvature of the corneal surface and the radius of the annular image.

Table 5. Measurement Accuracy ($A$) of Optical System for Corneas with Different Radii of Curvature ($r$)

| | | | | | | | |
|---|---|---|---|---|---|---|---|
| $r$(mm) | 5.5 | 6 | 7 | 7.8 | 9 | 10 | 11 |
| $A$(D) | 0.156 | 0.122 | 0.096 | 0.072 | 0.054 | 0.044 | 0.036 |

curve in the calculation of the radius of curvature of the corneal surface. With more sample data, the calibration curve could provide higher accuracy. In this research, 2.1 μm (0.56 pixel) is considered as the minimum variation of the radius of the image. With this value, the accuracy of the optical system for different radii of curvature of corneal surfaces can be obtained from the calibration curve. Results are listed in Table 5. It can be seen that for the steepest ($r = 5.5$ mm) and the flattest ($r = 11$ mm) corneal surfaces, the accuracy of the system, $A$, is 0.156D and 0.036D, respectively. The accuracy is 0.072D for the corneal surface with radius of curvature of 7.8 mm.

To verify the accuracy provided by the calibration curve, we investigate the variation of the radius of the annular image for three typical cases of corneal surface, by ZEMAX and TracePro software. The results are listed in Table 6, where $r$ is the radius of curvature of the corneal surface, $P$ is the corresponding corneal refraction, $\Delta P$ is the variation of corneal refraction according to Table 5, $R$ is the radius of the annular image, and $\Delta P'$ is the variation of corneal refraction calculated based on the calibration curve of Fig. 6. It can be seen that the calculated values of $\Delta P'$ are in good agreement with the actual values of $\Delta P$. Figure 7 shows the irradiance maps of the annular images provided by TracePro software.

The noise influence on the accuracy of the keratometer, including CCD detector noise and stray light noise of the optical system, is investigated by simulation with MATLAB. In practice, it is not difficult to eliminate the stray light of the imaging system to a level of 3%. The signal-to-noise ratio (SNR) of the CCD detector could be 48 dB. We add the stray light noise and CCD detector noise of the above values to the image signal, and calculate the radius of the annular image by the centroid algorithm. The corneal refraction is then obtained by the calibration curve shown in Fig. 6. It is shown that the deviation of the corneal refraction is about

Table 6. Verification Result of Accuracy[a]

| | | | | | | |
|---|---|---|---|---|---|---|
| $r$(mm) | 5.5 | 5.514 | 7.8 | 7.813 | 11 | 10.987 |
| $P$(D) | 61.364 | 61.208 | 43.269 | 43.197 | 30.682 | 30.718 |
| $\Delta P$(D) | 0.156 | | 0.072 | | 0.036 | |
| $R$(mm) | 0.7738 | 0.7763 | 1.1363 | 1.1387 | 1.6787 | 1.6764 |
| $\Delta P'$(D) | 0.177 | | 0.085 | | 0.037 | |
| $\Delta P'-\Delta P'$(D) | 0.021 | | 0.013 | | 0.001 | |
| $\lvert\Delta P'-\Delta P\rvert/\Delta P$ | 13% | | 18% | | 3% | |

[a] $r$ is the radius of curvature of the cornea, $P$ is the refractive power, $R$ is the radius of the annular image, $\Delta P$ is the actual variation of corneal refraction, and $\Delta P'$ is the calculated value of variation.

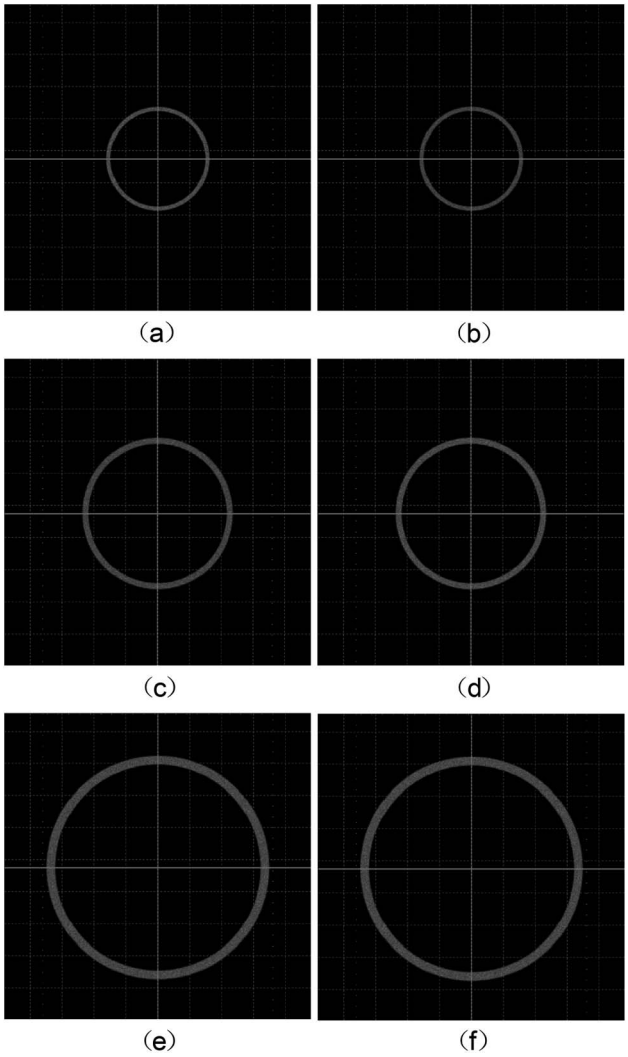


Fig. 7. Irradiance maps of annular images. (a) $r = 5.5$ mm, (b) $r = 5.514$ mm, (c) $r = 7.8$ mm, (d) $r = 7.813$ mm, (e) $r = 11$ mm, and (f) $r = 10.987$ mm.

0.002D from the value in the case without noise at radius of curvature of 7.8 mm.

In practice, the measurement accuracy is also affected by the status of subjects, such as incorrect position of the eye and incorrect staring at the fixation target. These are not further discussed in this paper.

To simulate the corneal astigmatism, we set the corneal surface with maximum and minimum refractions in two vertical meridians. In ZEMAX, the radius of curvature of the corneal surface in the $X$ (horizontal) direction is set to be 7.800 mm, and in the $Y$ (vertical) direction to be 7.938 mm. In this case, the cylindrical refraction of the corneal surface is 0.75D. Due to the astigmatism, the annular object can be focused only along the radial direction, either horizontal or vertical, at two specific planes. Figure 8 shows the irradiance maps of the annular images provided by TracePro software, where (a) is well-focused in the horizontal direction and (b) is well-focused in the vertical direction. The irradiance maps

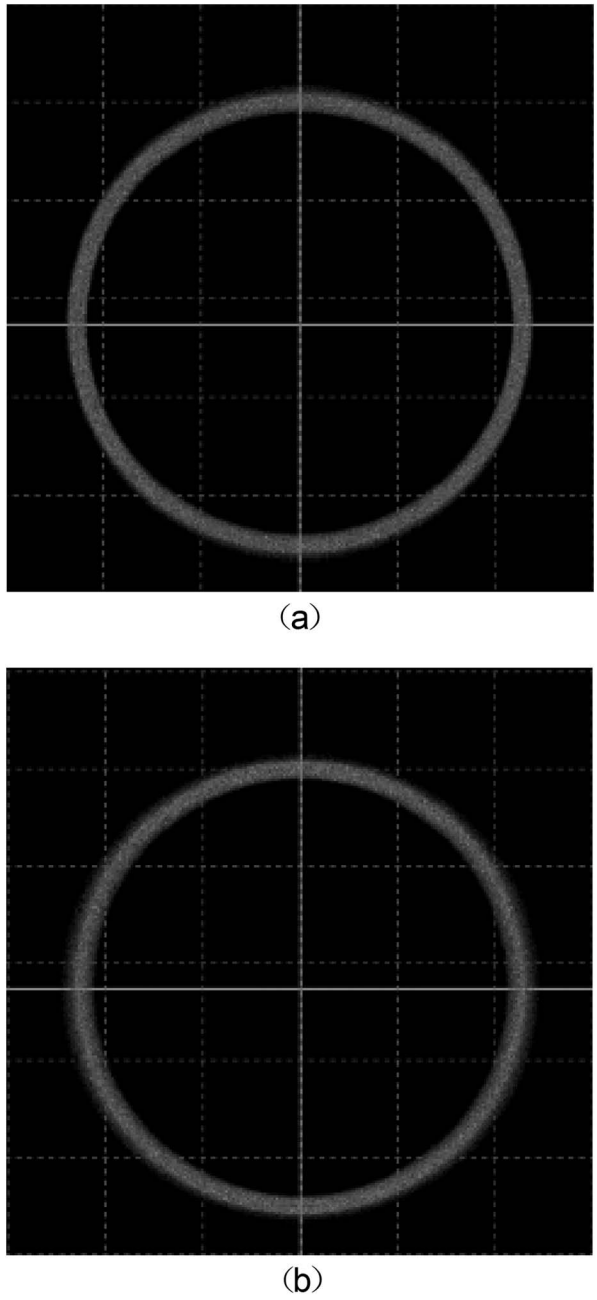


Fig. 8. Irradiance map of image in the case of cornea with astigmatism.

are used to calculate the radii of annular images. Then the refractions of the principal meridians of the corneal surface are obtained with the calibration curve, which is 43.279D and 42.578D, respectively. The calculated cylindrical refraction is then 0.70D, which is 0.05D lower compared with the expected value.

## 4. Conclusions

A novel high-accuracy imaging keratometer is proposed, and the corresponding optical system, consisting of an annular object, a first and a second imaging subsystem, and a CCD detector, is designed. It is demonstrated that the measurement range is about

30D–60D (5.5–11 mm in radius of curvature). The calibration curve of the apparatus is established with 12 sample radii of curvature of the corneal surface. Based on the calibration curve, the accuracies of the optical system at three typical radii of curvature are calculated. In the cases of the steepest ($r = 5.5$ mm) and the flattest ($r = 11$ mm) corneal surfaces, the accuracy is 0.156D and 0.036D, respectively. It is 0.072D for the corneal surface with radius of curvature of 7.8 mm. The measurement accuracy of corneal astigmatism is verified by setting the corneal surface with a cylindrical refraction of 0.75D, and it is shown that the measurement error is 0.05D. The external focusing model is adopted, with the position of the image plane and the image size varying as the radius of curvature of the corneal surface. The imaging keratometer has the advantages of modern optoelectronic imaging technology and image processing technology, and also has high accuracy and a wide measurement range.

This work is supported by the National Nature Science Foundation of China (No. 81170873) and the National Nature Science Foundation of China (No. 11104149).

## References

1. J. Liang, B. Grimm, S. Goelz, and J. F. Bille, "Objective measurement of wave aberrations of the human eye with the use of a Hartmann–Shack wave-front sensor," J. Opt. Soc. Am. A **11**, 1949–1957 (1994).
2. S. MacRae, R. R. Krueger, and R. A. Applegate, *Customized Corneal Ablation: The Quest for Supervision* (Slack, 2001).
3. J. F. Bille, C. F. H. Harner, and F. F. Loesel, *Aberration-Free Refractive Surgery: New Frontiers in Vision* (Springer, 2002).
4. J. Lee, "Wavefront technology for spectacle lenses," Rev. Ophthalmol. **12**(3), 91 (2005).
5. W. H. Seiple and J. P. Szlyk, "Clinical investigation into the vision performance provided by the iZon spectacle lens system," Rev. Ophthalmol. **145**(2), 1 (2008).
6. L. N. Thibos, X. Hong, A. Bradley, and R. A. Applegate, "Accuracy and precision of objective refraction from wavefront aberrations," J. Vision **4**(4), 329–351 (2004).
7. J. He, J. Gwiazda, F. Thorn, and R. Held, "Wave-front aberrations in the anterior corneal surface and the whole eye," J. Opt. Soc. Am. A **20**, 1155–1163 (2003).
8. H. Guo, Z. Wang, Q. Zhao, W. Quan, and Y. Wang, "Individual eye model based on wavefront aberration," Optik **116**, 80–85 (2005).
9. R. Gutmark and D. L. Guyton, "Origins of the keratometer and its evolving role in ophthalmology," Surv. Ophthalmol. **55**, 481–497 (2010).
10. S. B. Hannush, S. L. Crawford, G. O. Waring III, M. C. Gemmill, M. J. Lynn, and A. Nizam, "Accuracy and precision of keratometry, photokeratoscopy, and corneal modeling on calibrated steel balls," Arch. Ophthalmol. **107**, 1235–1239 (1989).
11. Z. Liu, A. Huang, and S. Pflugfelder, "Evaluation of corneal thickness and topography in normal eyes using the Orbscan corneal topography system," Br. J. Ophthalmol. **83**, 774–778 (1999).
12. J. G. Pérez, A. Cerviño, M. J. Giraldez, M. Parafita, and E. Yebra-Pimentel, "Accuracy and precision of EyeSys and Orbscan systems on calibrated spherical test surfaces," Eye Contact Lens **30**, 74–78 (2004).
13. B. Lackner, G. Schmidinger, S. Pieh, M. A. Funvoics, and C. Skorpik, "Repeatability and reproducibility of central corneal thickness measurement with Pentacam, Orbscan, and ultrasound," Optom. Vis. Sci. **82**, 892–899 (2005).
14. Y. Sun, S. Duthaler, and B. J. Nelson, "Autofocusing in computer microscopy: selecting the optimal focus algorithm," Microsc. Res. Tech. **65**, 139–149 (2004).
15. D. A. Atchison and G. Smith, "Chromatic dispersions of the ocular media of human eyes," J. Opt. Soc. Am. A **22**, 29–37 (2005).